Flooding Control by Electrochemically Reduced Graphene Oxide Additives in Silver Catalyst Layers for CO2 Electrolysis

Wu, Yuming; Idros, Mohamed Nazmi; Feng, Desheng; Huang, Wengang; Burdyny, Thomas; Wang, Bo; Wang, Geoff; Li, Mengran; Rufford, Thomas E.

DOI
10.1021/acsami.4c09095

Publication date
2024

Document Version
Final published version

Published in
ACS Applied Materials and Interfaces

ACS APPLIED MATERIALS & INTERFACES

www.acsami.org

Research Article

Flooding Control by Electrochemically Reduced Graphene Oxide Additives in Silver Catalyst Layers for CO_2 Electrolysis

Yuming Wu, Mohamed Nazmi Idros, Desheng Feng, Wengang Huang, Thomas Burdyny, Bo Wang, Geoff Wang, Mengran Li,* and Thomas E. Rufford*

Cite This: *ACS Appl. Mater. Interfaces* 2024, 16, 56967−56974

Read Online

ACCESS | Metrics & More | Article Recommendations | Supporting Information

ABSTRACT: Electrolyte flooding in porous catalyst layers on gas diffusion electrodes (GDE) limits the stability and high-current performance of CO_2 and CO electrolyzers. Here, we demonstrate the in situ electroreduction of graphene oxide (GO) to reduced graphene oxide (r-GO) within a silver catalyst layer on a carbon GDE. The r-GO introduces hydrophobicity regions in the catalyst layer that help mitigate electrolyte flooding during high current density CO_2 electrolysis to CO. The flooding-resistant r-GO/Ag-coated GDE achieves a sustained Faradaic efficiency of CO at 94% for more than 8 h, compared to a rapid drop from 95% to 66% in an Ag-coated GDE without r-GO at 100 mA·cm^{-2}. We found that GO enhances the electrochemically active surface area of the catalyst layer during CO_2 electrolysis tests because the incorporation of GO increases the roughness of the catalyst layer. The in situ method of electrochemically reducing GO to r-GO provides a low-cost, practical approach that can be applied during standard spray-deposition procedures to develop flooding-resistant GDEs.

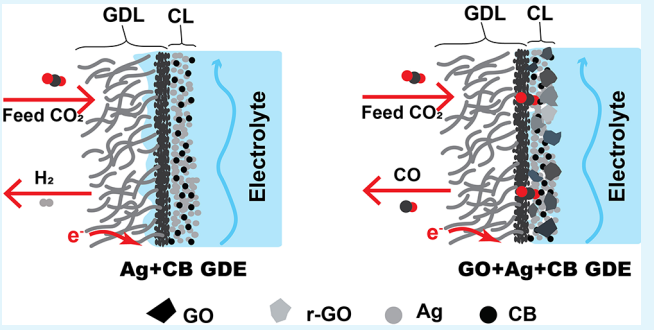

KEYWORDS: *CO_2 electrolysis, graphene oxide, gas diffusion electrode, flooding, electrolyzer*

INTRODUCTION

Electrochemical CO_2 reduction, or CO_2 electrolysis, is a promising approach to reducing carbon dioxide emissions by converting industrial CO_2 into value-added products.[1−3] The CO_2 electrolysis configurations closest to industrial deployment[4,5] use gas diffusion electrodes (GDEs) to support high surface area catalyst layers and minimize mass transfer resistance for the diffusion of CO_2 from the gas phase to the liquid electrolyte-catalyst interface.[6] A GDE typically comprises a carbon-based gas diffusion layer (GDL) coated with a porous catalyst layer. This catalyst layer (CL) commonly contains nanoparticles of the active catalysts, a polymer that acts as a binder and ionomer, and carbon black particles to improve the electrical conductivity of the layer.[7,8] State-of-the-art GDE-based electrolyzers can achieve high selectivity for CO at industrially relevant current densities (>200 mA·cm^{-2}).[9,10] However, practical applications are limited by the stability of the electrolyzer performance at a high current density.

A critical factor that leads to the degradation of CO_2 electrolyzer performance in extended high current density operation is the flooding of liquid electrolyte in the pores of the GDE.[11,12] Liquid ingress through the electrode can block CO_2 gas diffusion pathways to the catalyst sites, which impacts selectivity, and lead to carbonate salt precipitation across the electrode.[13] Electrode flooding occurs over short periods as carbon surfaces in the catalyst layer and supporting GDL lose hydrophobicity under applied potential due to electrowetting phenomena.[11,14−16] We note that polymer-based GDLs, such as those made from polytetrafluoroethylene (PTFE), are reported in lab-based studies to be flooding resistant GDEs, due to the highly hydrophobic nature of these fluorinated polymers.[10,17] However, the low conductivity of PTFE-based GDEs[18] has limited their scalability because nonconductive GDEs must rely on in-plane current distribution through the thin catalyst layer. As a result, PTFE and polymer-based GDLs have been limited to sizes of 1−5 cm^2 in published CO_2 electrolyzer studies.[17,19] In contrast, carbon-based GDLs have already been demonstrated at commercial scales in fuel cells, hydrogen electrolyzers, and flow cell batteries.

When focusing on the catalyst layer, the wetting behavior of the catalyst surface significantly impacts the performance of the GDE within an electrolyzer.[11,12] Several approaches have been investigated to mitigate flooding in the catalyst layer. A common approach in fuel cells and CO_2 electrolyzers is to add

Received: June 3, 2024
Revised: August 26, 2024
Accepted: August 28, 2024
Published: October 11, 2024

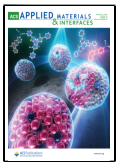

hydrophobic fluoropolymer particles, such as fluoroalkyl silane[20] or PTFE,[21,22] to the catalyst layer. There are comprehensive studies on the effects of PTFE additives on different layers in the gas diffusion layer. For example, Kim et al.[23] reported the effect of PTFE addition in the microporous layer (MPL) on the performance of GDE, while Shi et al.[22] investigated the CO_2 electrolysis on a PTFE-modified carbon fiber substrate. Nwabara et al.[24] studied the inclusion of PTFE particles in a silver-based catalyst layer, reporting that the addition of 5 wt % PTFE for CO_2 electrolysis results in a lower current density at all potentials compared to the other binders (e.g., Nafion and Sustainion) due to the poor electrical conductivity of PTFE.

Nonconductive fluoropolymers can retain hydrophobicity under applied electric potentials. However, the poor electrical conductivity of PTFE and similar fluoropolymer additives can (1) reduce the electrochemically active surface available for the reactions,[21,22] and (2) increase the cathode potential required at high-rate CO_2 conversion, which may impact the overall energy efficiency of the process.[24] Here, we demonstrate reduced graphene oxide (r-GO) as an additive material to the catalyst layer (Figure 1a) that is more electrically conductive

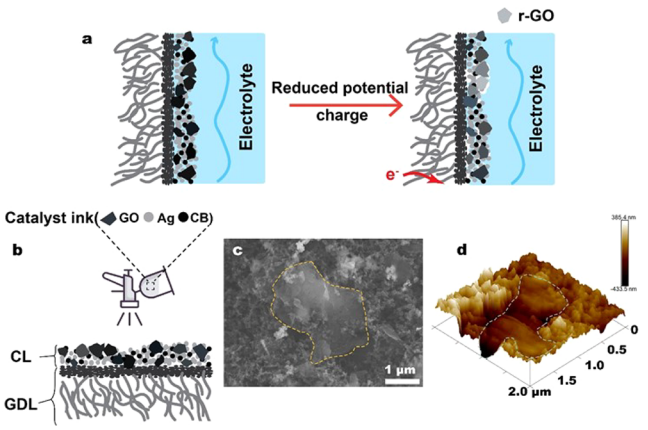

Figure 1. (a) Schematic of the adjustment of GDE wettability through in situ electroreduction of GO to mitigate electrolyte flooding during CO_2 electrolysis; (b) process of spraying the catalyst ink on a commercial carbon-based GDL; (c) SEM image and (d) AFM topography of the catalyst layer on GO+Ag+CB GDE.

than fluoropolymers but still provides a hydrophobic nature to catalyst layers for flooding resistance. Our approach builds on the work of Song et al.[25] and Zhang et al.,[26] who reported a reduction of GO to a hydrophobic r-GO by electrochemical methods for other applications. Studies on the performance of GDEs in fuel cells have previously reported that the addition of r-GO can improve fuel cell performance,[27] but this has not been reported for CO_2 electrolyzers, and in the fuel cell study, the r-GO was added to the microporous layer of the GDL, not the catalyst layer.

To confirm the electroreduction condition required in the electrolyzer, we deposited a thin film of GO flakes (Figure S1) on a glassy carbon electrode. Then we performed cyclic voltammetry and constant potential bulk electrolysis tests in an aqueous $KHCO_3$ electrolyte (Figure S2a) to identify the reduction onset potentials. The CV profile of the GO thin film shows a notable peak at −1.2 V versus AglAgCl in the cathodic sweep from −0.2 to −1.5 V. The Raman spectra in Figure S2c following an electroreduction treatment for 10 min (in Figure S2b), indicate the degree of reduction of graphene oxide.[28,29] The XPS spectra in Figure S2d provide consistent evidence of electrochemical reduction of the GO to r-GO with an increase in the atomic ratio of the C−C group.

We then test a hypothesis that GO particles mixed into a catalyst layer can be reduced to r-GO under CO_2 electrolysis conditions to create a flooding-resistant catalyst layer on a GDE (Figure 1a). For high current density applications, a key advantage of r-GO compared to other hydrophobic additives, such as PTFE,[30] fluorinated silane,[20,22] or fluorinated ethylene propylene,[31] is that the electrical conductivity of reduced graphene oxide flakes ($6.2 \times 10^2 - 6.2 \times 10^3$ S m^{-1})[32] is many orders of magnitude higher than the conductivity of materials like PTFE (less than 6×10^{-17} S m^{-1}).[18] We prepared the r-GO/Ag GDE by spraying an ink of GO, Ag nanoparticles, carbon black (CB), and Nafion in 2-propanol onto a commercial gas diffusion layer (Figure 1b). The compositions of the catalyst layers that we prepared are listed in Table 1.

Table 1. Compositions of Catalyst Inks

	GO/ mg	Ag particles/ mg	Carbon black/mg	Nafion/ mL	Isopropanol/ mL
GO+Ag +CB	10	50	40	0.5	2
Ag+CB	N/A	50	50	0.5	2
GO+CB	50	N/A	50	0.5	2
GO+Ag	50	50	N/A	0.5	2

Scanning electron microscopy (SEM) in Figure 1c shows a representative GO flake in the Ag catalyst layer on the carbon GDL. The GO is evenly distributed as flakes with a lateral size of 1−2 μm (consistent with SEM and TEM of GO in Figure S1) among nanoparticles with a size distribution from 30 to 100 nm. Atomic force microscopy (AFM) results (Figure 1d) provide further information about the morphology and roughness of the GO-embedded catalyst layer.

To evaluate the performance of the GO+Ag+CB GDE, we performed CO_2 electrolysis measurements at current densities from 100 mA·cm^{-2} using the liquid flow cell electrolyzer described in the following experimental methods and our previous work.[30] For control experiments, we prepared a cathode electrode Ag+CB GDE with catalyst layers containing the same ionomer and silver and carbon black only (see the compositions in Table 1).

EXPERIMENTAL METHODS

Electroreduction of GO to r-GO: A suspension composed of 20 mg of GO (15−20 sheets, Sigma-Aldrich Pty Ltd., see Figure S1) in 4 mL of isopropyl alcohol (IPA, ≥ 99.7%, Sigma-Aldrich) was sonicated for 1 h and then dropped by a pipette onto one side of a glassy carbon plate (Carbon-Vitreous-3000C − Foil, 10 mm × 10 mm). The GO loading was 0.5 ± 0.1 mg.cm^{-2}, confirmed by gravimetric analysis after evaporation of the IPA. The dried electrode was the working electrode for demonstrating GO electrocution solely.

The electroreduction measurements of GO were conducted in a three-electrode cell composed of a glass carbon plate as the cathode with active electrode area 1.5 cm^2, AglAgCl (ALS Co., Ltd.) as the reference, and Pt wire as the anode. 0.1 M $KHCO_3$ (≥99.5%, Sigma-Aldrich) was the electrolyte. A potentiostat charged and controlled the cell (PGSTAT204, Metrohm Autolab). Cyclic voltammetry (CV) was performed at a scan

https://doi.org/10.1021/acsami.4c09095
ACS Appl. Mater. Interfaces 2024, 16, 56967−56974

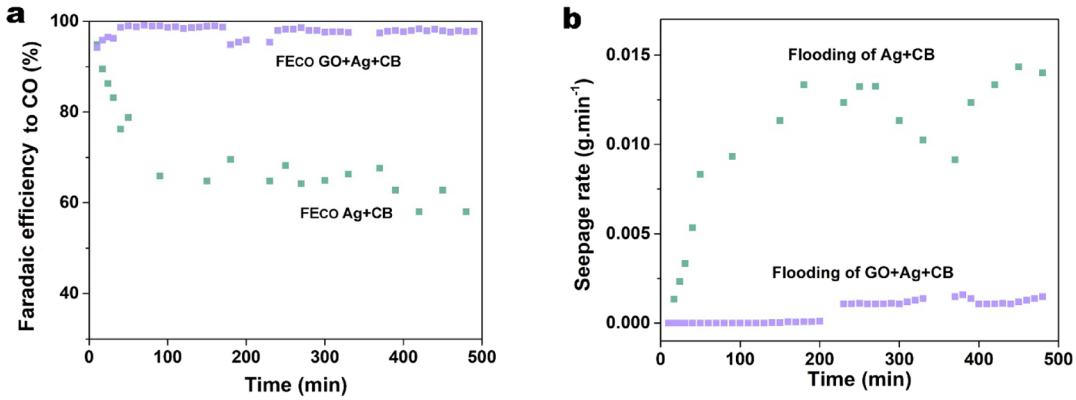

Figure 2. (a) Selectivity for CO and (b) real-time seepage rate for Ag+CB GDE and GO+Ag+CB GDE during an 8-h CO_2 electrolysis test at a current density of 100 mA·cm^{-2} (data around 210 and 350 min was missing due to an adjustment of the GC autoinjection program).

rate 50 mV/s. The electroreduction (chronoamperometry) treatment involved applying a potential of −1.2 V vs AglAgCl at a given time.

Electrochemical CO_2 reduction measurements: The catalyst layer was spray coated on the MPL side of a commercial GDL (W1S1010 with MPL, 410 μm, *Fuel Cell Store*). Gas permeability and sheet resistance on the specification are 13.71 × 10^{-12} and 13 mΩ·cm^2, respectively. The catalyst composition is included in a prepared ink. Table 1 lists the compositions of four catalyst inks. The information on materials and reagents in Table 1 is listed: GO (15−20 sheets, Sigma-Aldrich Pty Ltd., see Figure S1); Ag particles (Ag, 99.9%, 20−40 nm, Thermo Fisher Scientific); carbon black (CB, 99%, Thermo Fisher Scientific); Nafion (5 wt % perfluorinated resin, Sigma-Aldrich); isopropanol (IPA, ≥ 99.7%, Sigma-Aldrich). After sonication for 30 min, inks were sprayed onto the MPL using an airbrush (RS PRO Air Brush Kit, with 0.3 mm Tip) with a fixed airflow. The electrodes were dried at 90 °C to evaporate the IPA and water. The loadings of the catalyst layer with various components were constant (1.0 ± 0.1 mg cm^{-2}), confirmed by gravimetric analysis before and after the spray coating.

CO_2 electrolysis measurements were performed in a custom-made flow cell (Figure S9).[30] A potentiostat charged and controlled the electrolyzer (Metrohm Autolab PGSTAT302N). The AgNP-decorated GDE served as the cathode, a 6 mm thick nickel foam (99.5%, Goodfellow Cambridge Limited) was used as the anode, and AglAgCl was used as the reference electrode. Nafion 117 membrane (from FuelCell Store) was adopted to separate the two chambers. The applied cathode area facing the catholyte was 1 × 1 cm^2. A 0.1 M $KHCO_3$ (≥99.5%, Sigma-Aldrich) aqueous solution as catholyte was pumped into the cathode chamber in a single pass at a flow rate of 2 mL/min. A 500 mL 1 M KOH (≥85%, pellets, Sigma-Aldrich) aqueous solution was circulated in the anode chamber at 10 mL/min. During stability tests, the anolyte was renewed every 10 h. A mass flow controller regulated the flow rate of influent CO_2 at 60 sccm. Each current density was applied for 600 s before injecting the outgas to a gas chromatograph (Shimadzu GC-2030, more setting details in the Supporting Information) and collecting the liquid product from the effluent catholyte. The effluent catholyte was analyzed using nuclear magnetic resonance (NMR) ^{1}H spectroscopy (Bruker Avance 500 high-resolution NMR; more details about product analysis and calculations are provided in the Supporting Information). Meanwhile, the electrolyte seepage rate was determined by measuring the mass of the collected seeping catholyte at a given time, as reported previously.[33]

Characterization of materials: Scanning electron microscopy (SEM) and energy-dispersive X-ray spectroscopy (EDS) were performed on a JEOL JSM-7001F instrument. Transmission electron microscopy (TEM, Hitachi HT 7700) was employed to acquire the morphology of GO flakes. Bruker Dimension ICON AFM has been used to produce AFM images of the surface of catalyst layers. The ScanAsyst mode was utilized with the ScanAsyst-Air probe, which has a spring constant of 0.4 N/m. NanoScope Analysis software was employed to analyze the AFM images and determine the average profile roughness. X-ray photoelectron spectroscopy (XPS) was conducted using a Kratos Axis Ultra XPS with a state-of-the-art Kratos Axis Ultra photoelectron spectrometer. Raman spectra were obtained by a Renishaw Raman microscope, using a laser source with a wavelength of 512 nm.

Sessile drop contact angles were measured using a goniometer designed by ourselves.[33] We determined the contact angles by analyzing the images with ImageJ. A 1−10 μL volume pipette was used to dispense 5 ± 0.2 μL of liquid at least three different locations on each sample surface. Prior to measuring, we disassembled the electrolyzer and immersed the GDE in deionized water to thoroughly remove residual electrolyte and precipitated salts from the whole GDEs. All of the samples were dried before the contact angle measurements.

The ECSA (ECSA = A·C_{dl}/loading$_{catalyst}$) was characterized by a C_{dl}-specific double-layer capacitance. C_{dl} was determined by performing ex situ CV in a single cell with three electrodes filled with 0.5 M $KHCO_3$. The CV was conducted at seven scan rates (0.06, 0.08, 0.1, 0.2, 0.3, 0.4, and 0.5 V·s^{-1}), as shown in Figures S10 and S11. The charging current density (taken at 0.906 V vs RHE, 0.08 V vs AglAgCl) was plotted versus the scan rate, where C_{dl} was calculated from the slope of this linear plot. Three ECSA measurements after each CO_2 electrolysis measurement time were tested and their average.

RESULTS AND DISCUSSION

Figure 2 demonstrates that the inclusion of GO in catalyst layer significantly alleviates electrolyte flooding, resulting in a stable and highly selective CO_2 electrolysis over 8 h. In Figure 2a, the Faradaic efficiency of CO (FE_{CO}) for the GO+Ag+CB GDE remains above 94% for more than 8 h at 100 mA·cm^{-2}. Conversely, the performance of the Ag+CB GDE deteriorates

https://doi.org/10.1021/acsami.4c09095
ACS Appl. Mater. Interfaces 2024, 16, 56967−56974

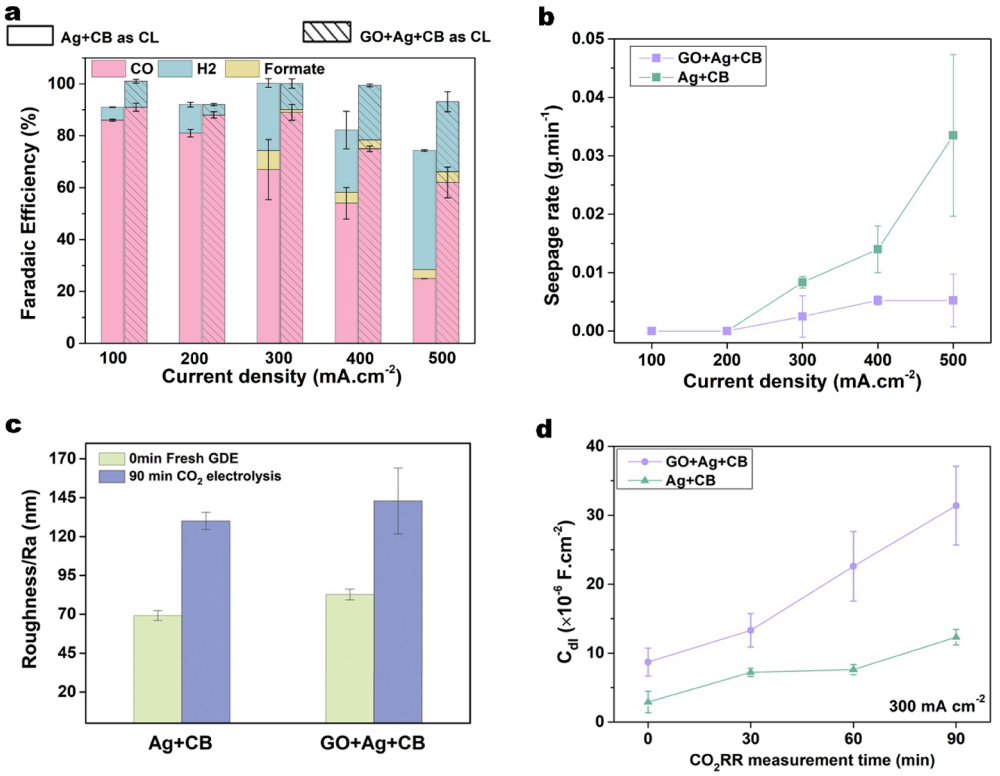

Figure 3. (a) Faradaic efficiency of the detectable CO, H_2, and formate for Ag+CB and GO+Ag+CB GDEs; (b) average rate of catholyte seepage through the GDEs; (c) change of average profile roughness (Ra, obtained by the analysis of AFM image) on the two catalyst layers after 90 min of CO_2 electrolysis at 300 mA·cm^{-2}; (d) specific double layer of GDEs with the two catalyst layers before and after CO_2 electrolysis at 300 mA·cm^{-2} for 30, 60, and 90 min. C_{dl} was calculated from the electrochemical surface area described in the Supporting Information. The error bars on FEs in (a) represent the standard deviation of three measurements of effluent gas compositions. The error bars in parts (b, c, and d) represent the standard deviation of three independent measurements on various GDEs for each measured current density and time.

rapidly within the first 100 min, with FE_{CO} dropping from 95% to 66%, accompanied by a noticeable rise in the electrolyte seepage rate (see Figure 2b). The seepage rate was measured to quantify the electrolyte flooding by measuring the mass of collected seeping catholyte as reported earlier.[33] By virtue of the in situ reduction of GO in the catalyst layer under electrolyzer conditions, the exclusive stability of the GO+Ag+CB GDE is established through effective control of electrolyte flooding.

We note in Figure 2 an increase in FE_{CO} of GO+Ag+CB in the first 60 min of the stability test. This initial performance increase might be attributed to the time required for electrochemical reduction of the GO to hydrophobic r-GO. Over an extended operating time of 60 h, the stability of the GO+Ag+CB GDE was demonstrated, with FE_{CO} only declining to 77% after the prolonged operation (Figure S4). At end of the 60-h test, the seepage rate in the GO+Ag+CB GDE remains at 0.0014 g·min^{-1}, similar to the rate observed during the first 8-h test (Figure 2b). We acknowledge that these stability tests are much shorter than the several thousand hours of stable operation required for industrial CO_2 electrolyzers. Still, these results highlight the potential of using GO as a superior wet-proofing additive within GDEs in CO_2 electrolyzers to mitigate electrolyte flooding and uphold CO_2 diffusion pathways.

To fully evaluate the performance of the GO+Ag+CB GDE, additional CO_2 electrolysis measurements were performed at current densities from 100 to 500 mA·cm^{-2}. Fresh GDEs were used at each current density to avoid any cumulative effects of electrolyte flooding or catalyst surface changes that might occur during electrochemical measurements. Figure 3a shows that the GO+Ag+CB GDE significantly impacts the distribution of cathode products at high current densities compared to the Ag+CB GDE control experiment . The primary products in each set of tests are CO and H_2, but low concentrations of formate products are detected in the catholyte liquid at high current densities. At a current density of 100 mA·cm^{-2}, the selectivity for CO for both electrodes falls within the typical range of FE_{CO} = 90−95% for Ag nanoparticle catalysts on carbon GDEs, as reported in similar experiments.[12,30,33,34] When the current density increases to 300 mA·cm^{-2} and higher, there are significant differences in both FE_{CO} and FE_{H2} (Figure 3a) and electrolyte seepage rates (Figure 3b) between the Ag+CO electrode and the GO-embedded electrode. The seepage rate of the Ag+CB electrode increases from nearly zero at 100 mA·cm^{-2} to 0.034 ± 0.014 g·min^{-1} at 500 mA·cm^{-2}, which indicates severe electrolyte flooding at high current density.[33] When the flooded electrolyte impedes the supply of CO_2 in the Ag+CB GDE, a drop occurs in FE_{CO} to less than 30% at 500 mA·cm^{-2} with rising H_2 evolution and a limiting CO_2 reduction current density of 233 mA·cm^{-2} for CO at 400 mA·cm^{-2} (Figure S6).

In contrast, the GO-embedded catalyst layer in the GO+Ag+CB GDE exhibits stable CO selectivity up to 300 mA·cm^{-2} (FE_{CO} = 88%) (Figure 3a) and then a fall to only FE_{CO} = 62% at 500 mA·cm^{-2}. The observed degradation of FE_{CO} for the GO-embedded catalyst layer at current densities above 200 mA·cm^{-2} is remarkably less than that of other carbon-based

https://doi.org/10.1021/acsami.4c09095
ACS Appl. Mater. Interfaces 2024, 16, 56967−56974

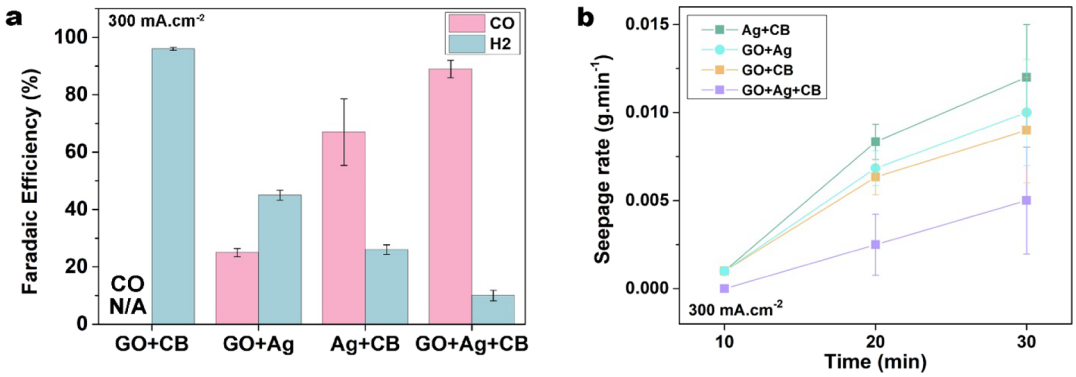

Figure 4. (a) Selectivity and (b) seepage rate of GDEs with different components in the catalyst layer charged at 300 mA·cm^{-2} (see Table 1 for the details of composition). The error bars on FEs in (a) represent the standard deviation of three measurements of effluent gas compositions. The error bars on seepage rates in (b) represent the standard deviation of three independent measurements on different GDEs for each measured current density.

GDEs. For example, Wei et al.[35] reported a FE_{CO} fall from 95% at 200 mA·cm^{-2} to only 32.7% at 300 mA·cm^{-2} with a Ag catalyst in a similar experiment to ours. We attribute the excellent stability of the GO+Ag+CB electrode to the wetting resistance of GO reduced to r-GO in the catalyst layer under electrolyzer conditions. This conclusion is supported by the very low seepage rate in the GO+Ag+CB electrode, which remains less than 0.005 ± 0.005 g·min^{-1} at 500 mA·cm^{-2} (seven times lower seepage rate than in the Ag+CB GDE).

We note that the sum of FEs for the CO, H_2, and formate products is greater than 90% for both electrodes and 100, 200, and 300 mA·cm^{-2}, which is within the typical uncertainty of these measurements. However, we observed a more significant gap in the electron balance (Figure 3a) at current densities higher than 300 mA·cm^{-2}. This experimental observation is due to the H_2 bubbles pumped out with catholyte.[33] Such imperfection in the electrolyzer is related to the imbalanced gas/liquid pressures across the GDE. The phenomenon of less than 100% FE is a common issue for other studies.[36,37]

To investigate the mechanism of the overall enhanced performance of CO_2 electrolysis, we performed a series of CO_2 electrolysis experiments with the GO+Ag+CB and Ag+CB GDEs at different electrolysis time durations. We measured surface roughness of the catalyst layer by AFM (Figures 3c and S7) and electrochemically active surface area (ECSA) (Figure 3d) of the GDE before and after the CO_2 electrolysis at 300 mA·cm^{-2} for various time durations. Figure 3c shows that after CO_2 electrolysis, the surface roughness of both catalyst layers is almost double their initial roughness, which may be due to the surface restructuring of the silver during electrolysis.[38] Figure 3d compares the double-layer capacitances (C_{dl}) of the GO +Ag+CB and Ag+CB electrodes before and after electrolysis. The double-layer capacitance is a function of ECSA of the electrode, providing information on charge capacity and kinetics.[39] The addition of GO prior to CO_2 electrolysis in Figure 3d enhances the ECSA, possibly due to the more hydrophilic nature of GO compared to carbon black (as shown in Figure S3). GO's hydrophilic properties on the GO+Ag+CB GDE increase the surface area exposed to the electrolyte during ECSA measurements. After CO_2 electrolysis at 300 mA·cm^{-2}, the double-layer capacitances of both types of electrodes increases. The similar increasing trend on GDE has been observed by other researchers.[34] The escalating ECSA may be caused by the increased surface roughness observed in Figure 3c. This trend aligns with the findings of Jiang et al.[40] who noted that a rising ECSA trend is associated with a rougher electrode surface resulting from plasma pretreatment. This surface roughness and ECSA results suggest that the GO-embedded catalyst layer proves to have a more active surface area with increased time, which is consistent with the seepage and FE_{CO} results presented in Figure 3a and b.

To confirm the role of GO and r-GO in the catalyst layer, we evaluated two more GDEs with different catalyst layer formulations: (i) GO+Ag without carbon black and (ii) a control electrode of GO+CB without the Ag nanoparticles, while the same ionomer is contained in each catalyst layer, as provided in Table 1. As expected,[41,42] we did not detect any CO_2 reduction products in the GO+CB experiment without silver on the cathode (Figure 4a). Hence, GO/r-GO is not able to provide active sites for CO_2 reduction, despite the inclusion of GO effectively alleviate the electrolyte flooding throughout the CO2 electrolysis (see Figure 4b). The performance in Figure 4a further demonstrates that GO flakes cannot entirely replace carbon black because GO+Ag only achieved FE_{CO} 25% at 300 mA·cm^{-2}. The role of CB in the catalyst layer has been reported as a suitable dispersant for the catalyst materials by Zheng et al.[43] We also observed the well-dispersed silver particles surrounded by CB (see Figure S8a), while the SEM images in Figure S8b show that Ag nanoparticles tend to agglomerate around the GO flakes in GO+Ag GDE. Further, the layer-by-layer GO stacking structure in the GO+Ag electrodes may inhibit through-plane gas diffusion to the catalyst layers.[44]

Meanwhile, the seepage rate of the GO+Ag GDE does not decrease as expected with the transition from GO to r-GO. The higher seepage rate compared to the GO+Ag+CB GDE might be due to the increased potential at the GO+Ag GDE, as shown in Figure S5. An increase in electrode potential can result in stronger electrowetting,[45] where the liquid spreads more easily across the solid surface under a higher applied electric field.[11] This enhanced electrowetting significantly contributes to electrolyte flooding in the GO+Ag GDE.

These findings suggest that there is likely an optimal ratio of GO to CB in the catalyst layer to balance the wettability and porosity effects. Optimization of the catalyst ink formulation is beyond the focus of this paper but could be an essential topic to explore in detail for improved fabrication of cathodes for CO_2 electrolyzers.

https://doi.org/10.1021/acsami.4c09095
ACS Appl. Mater. Interfaces 2024, 16, 56967−56974

CONCLUSIONS

In summary, we exploited the hydrophilicity to hydrophobicity transition between GO and r-GO through the in situ electroreduction of GO on GDE in a CO_2 electrolyzer. This reduction helps mitigate electrolyte flooding and maintain diffusion paths for CO_2 in the GDE. The CO_2 electrolysis measurements show that FE_{CO} maintains at 89% at 300 mA·cm^{-2}. At the same time, the C_{dl} of the GDE increases with the incorporation of GO, thanks to the increased roughness of the CL surface compared to a control GDE without GO. Owing to these advantages, the GO-incorporated GDE could persistently produce CO above 94% FE for up to 8 h at 100 mA·cm^{-2}. We showcase the effectiveness of incorporating GO as an alternative strategy for future catalyst layer design in large-scale CO_2 electrolysis. Furthermore, we envisage a similar chemical transformation-induced wet-proofing effect of other 2D materials such as MoS_2[46] and MXene.[47]

ASSOCIATED CONTENT

Supporting Information

The Supporting Information is available free of charge at https://pubs.acs.org/doi/10.1021/acsami.4c09095.

Methodologies of measurement and analysis of electrochemical products; morphology of received GO and GDEs; electroreduction treatments on the received GO and related Reman and XPS characterizations; cathode potentials during the CO_2 electrolysis; AFM topography of GDEs; NMR spectrum of collected effluent catholyte; CV curves for ECSA measurements; Faradaic efficiency for CO and H_2 for the GO-embedded GDE in 60 h stability test; images of contact angles change after CO_2 electrolysis (PDF)

AUTHOR INFORMATION

Corresponding Authors

Mengran Li − *Department of Chemical Engineering, the University of Melbourne, Parkville, Victoria 3010, Australia;* orcid.org/0000-0001-7858-0533; Email: aaron.li1@unimelb.edu.au

Thomas E. Rufford − *School of Chemical Engineering, The University of Queensland, Brisbane, Queensland 4072, Australia; ARC Centre of Excellence for Green Electrochemical Transformation of Carbon Dioxide, The University of Queensland, Brisbane, Queensland 4072, Australia;* orcid.org/0000-0002-8865-7976; Email: t.rufford@uq.edu.au

Authors

Yuming Wu − *School of Chemical Engineering, The University of Queensland, Brisbane, Queensland 4072, Australia;* Present Address: School of Engineering, Macquarie University, Macquarie Park, NSW 2109; orcid.org/0000-0003-2809-0338

Mohamed Nazmi Idros − *School of Chemical Engineering, The University of Queensland, Brisbane, Queensland 4072, Australia*

Desheng Feng − *School of Chemical Engineering, The University of Queensland, Brisbane, Queensland 4072, Australia*

Wengang Huang − *School of Chemical Engineering, The University of Queensland, Brisbane, Queensland 4072, Australia*

Thomas Burdyny − *Materials for Energy Conversion and Storage (MECS), Department of Chemical Engineering, Faculty of Applied Sciences, Delft University of Technology, Delft 2629 HZ, The Netherlands;* orcid.org/0000-0001-8057-9558

Bo Wang − *Chair of Functional Materials, Department of Materials Science & Engineering, Saarland University, Saarbrücken 66123, Germany;* orcid.org/0000-0003-2270-2241

Geoff Wang − *School of Chemical Engineering, The University of Queensland, Brisbane, Queensland 4072, Australia*

Complete contact information is available at: https://pubs.acs.org/10.1021/acsami.4c09095

Notes

The authors declare no competing financial interest.

ACKNOWLEDGMENTS

This research received funding from the Australian Government through an ARC Linkage Project (LP160101729) and the ARC Centre of Excellence for Green Electrochemical Transformation of Carbon Dioxide (CE230100017). M.L. also acknowledges salary funding from the ARC through ARC fellowship DE230100637. Y.W. and M.N.I. received funding for PhD living stipends from the UQ Research Training Program (RTP) scholarship. We acknowledge the facilities and the scientific and technical assistance of the Microscopy Australia Facility at the Centre for Microscopy and Microanalysis (CMM), The University of Queensland. We thank Ms Ying Yu for the training and assitance of Raman spectroscopy. Authors appreciate Science Workshops at the University of Queensland for their assitance in installing pipeline of the gas chromatograph.

REFERENCES

(1) Whipple, D. T.; Kenis, P. J. A. Prospects of CO2 Utilization via Direct Heterogeneous Electrochemical Reduction. *J. Phys. Chem. Lett.* **2010**, *1* (24), 3451−3458.

(2) Bushuyev, O. S.; De Luna, P.; Dinh, C. T.; Tao, L.; Saur, G.; van de Lagemaat, J.; Kelley, S. O.; Sargent, E. H. What Should We Make with CO2 and How Can We Make It? *Joule* **2018**, *2* (5), 825−832.

(3) De Luna, P.; Hahn, C.; Higgins, D.; Jaffer, S. A.; Jaramillo, T. F.; Sargent, E. H. What would it take for renewably powered electrosynthesis to displace petrochemical processes? *Science* **2019**, *364* (6438), No. eaav3506.

(4) Vennekoetter, J.-B.; Sengpiel, R.; Wessling, M. Beyond the catalyst: How electrode and reactor design determine the product spectrum during electrochemical CO2 reduction. *Chem. Eng. J.* **2019**, *364*, 89−101.

(5) Wu, D.; Jiao, F.; Lu, Q. Progress and Understanding of CO2/CO Electroreduction in Flow Electrolyzers. *ACS Catal.* **2022**, *12* (20), 12993−13020.

(6) Garg, S.; Li, M.; Weber, A. Z.; Ge, L.; Li, L.; Rudolph, V.; Wang, G.; Rufford, T. E. Advances and challenges in electrochemical CO_2 reduction processes: an engineering and design perspective looking beyond new catalyst materials. *J. Mater. Chem. A* **2020**, *8* (4), 1511−1544.

(7) Weng, L.-C.; Bell, A. T.; Weber, A. Z. Modeling gas-diffusion electrodes for CO2 reduction. *Phys. Chem. Chem. Phys.* **2018**, *20* (25), 16973−16984.

(8) Nguyen, T. N.; Dinh, C.-T. Gas diffusion electrode design for electrochemical carbon dioxide reduction. *Chem. Soc. Rev.* **2020**, *49* (21), 7488−7504.

(9) Higgins, D.; Hahn, C.; Xiang, C.; Jaramillo, T. F.; Weber, A. Z. Gas-Diffusion Electrodes for Carbon Dioxide Reduction: A New Paradigm. *ACS Energy Lett.* **2019**, *4* (1), 317−324.
(10) García de Arquer, F. P.; Dinh, C.-T.; Ozden, A.; Wicks, J.; McCallum, C.; Kirmani, A. R.; Nam, D.-H.; Gabardo, C.; Seifitokaldani, A.; Wang, X.; et al. CO2 electrolysis to multicarbon products at activities greater than 1 A cm^{-2}. *Science* **2020**, *367* (6478), 661.
(11) Li, M.; Idros, M. N.; Wu, Y.; Burdyny, T.; Garg, S.; Zhao, X. S.; Wang, G.; Rufford, T. E. The role of electrode wettability in electrochemical reduction of carbon dioxide. *J. Mater. Chem. A* **2021**, *9* (35), 19369−19409.
(12) Yang, K.; Kas, R.; Smith, W. A.; Burdyny, T. Role of the Carbon-Based Gas Diffusion Layer on Flooding in a Gas Diffusion Electrode Cell for Electrochemical CO2 Reduction. *ACS Energy Lett.* **2021**, *6* (1), 33−40.
(13) Moss, A. B.; Garg, S.; Mirolo, M.; Giron Rodriguez, C. A.; Ilvonen, R.; Chorkendorff, I.; Drnec, J.; Seger, B. In operando investigations of oscillatory water and carbonate effects in MEA-based CO2 electrolysis devices. *Joule* **2023**, *7* (2), 350−365.
(14) Xu, Y.; Edwards, J. P.; Liu, S.; Miao, R. K.; Huang, J. E.; Gabardo, C. M.; O'Brien, C. P.; Li, J.; Sargent, E. H.; Sinton, D. Self-Cleaning CO2 Reduction Systems: Unsteady Electrochemical Forcing Enables Stability. *ACS Energy Lett.* **2021**, *6* (2), 809−815.
(15) Nwabara, U. O.; Cofell, E. R.; Verma, S.; Negro, E.; Kenis, P. J. A. Durable Cathodes and Electrolyzers for the Efficient Aqueous Electrochemical Reduction of CO2. *ChemSuschem* **2020**, *13* (5), 855−875.
(16) Leonard, M. E.; Orella, M. J.; Aiello, N.; Román-Leshkov, Y.; Forner-Cuenca, A.; Brushett, F. R. Editors' Choice-Flooded by Success: On the Role of Electrode Wettability in CO2 Electrolyzers that Generate Liquid Products. *J. Electrochem. Soc.* **2020**, *167* (12), 124521.
(17) Dinh, C.-T.; García de Arquer, F. P.; Sinton, D.; Sargent, E. H. High Rate Selective, and Stable Electroreduction of CO2 to CO in Basic and Neutral Media. *ACS Energy Lett.* **2018**, *3* (11), 2835−2840.
(18) Nishi, Y.; Iizuka, S.; Faudree, M. C.; Oyama, R. Electrical Conductivity Enhancement of PTFE (Teflon) Induced by Homogeneous Low Voltage Electron Beam Irradiation (HLEBI). *Mater. Trans.* **2012**, *53* (5), 940−945.
(19) Dinh, C.-T.; Burdyny, T.; Kibria, M. G.; Seifitokaldani, A.; Gabardo, C. M.; García de Arquer, F. P.; Kiani, A.; Edwards, J. P.; De Luna, P.; Bushuyev, O. S.; et al. CO2 electroreduction to ethylene via hydroxide-mediated copper catalysis at an abrupt interface. *Science* **2018**, *360* (6390), 783−787.
(20) Ma, W.; Xie, S.; Liu, T.; Fan, Q.; Ye, J.; Sun, F.; Jiang, Z.; Zhang, Q.; Cheng, J.; Wang, Y. Electrocatalytic reduction of CO2 to ethylene and ethanol through hydrogen-assisted C−C coupling over fluorine-modified copper. *Nat. Catal.* **2020**, *3* (6), 478−487.
(21) Xing, Z.; Hu, L.; Ripatti, D. S.; Hu, X.; Feng, X. Enhancing carbon dioxide gas-diffusion electrolysis by creating a hydrophobic catalyst microenvironment. *Nat. Commun.* **2021**, *12* (1), 136.
(22) Shi, R.; Guo, J.; Zhang, X.; Waterhouse, G. I. N.; Han, Z.; Zhao, Y.; Shang, L.; Zhou, C.; Jiang, L.; Zhang, T. Efficient wettability-controlled electroreduction of CO2 to CO at Au/C interfaces. *Nat. Commun.* **2020**, *11* (1), 3028.
(23) Kim, B.; Hillman, F.; Ariyoshi, M.; Fujikawa, S.; Kenis, P. J. A. Effects of composition of the micro porous layer and the substrate on performance in the electrochemical reduction of CO2 to CO. *J. Power Sources* **2016**, *312*, 192−198.
(24) Nwabara, U. O.; Hernandez, A. D.; Henckel, D. A.; Chen, X.; Cofell, E. R.; de-Heer, M. P.; Verma, S.; Gewirth, A. A.; Kenis, P. J. A. Binder-Focused Approaches to Improve the Stability of Cathodes for CO2 Electroreduction. *ACS Appl. Energy Mater.* **2021**, *4* (5), 5175−5186.
(25) Song, S.; Yang, H.; Su, C.; Jiang, Z.; Lu, Z. Ultrasonic-microwave assisted synthesis of stable reduced graphene oxide modified melamine foam with superhydrophobicity and high oil adsorption capacities. *Chem. Eng. J.* **2016**, *306*, 504−511.
(26) Zhang, Z.-H.; Chen, Z.-Y.; Tang, Y.-H.; Li, Y.-T.; Ma, D.; Zhang, G.-D.; Boukherroub, R.; Cao, C.-F.; Gong, L.-X.; Song, P.; et al. Silicone/graphene oxide co-cross-linked aerogels with wide-temperature mechanical flexibility, super-hydrophobicity and flame resistance for exceptional thermal insulation and oil/water separation. *J. Mater. Sci. Technol.* **2022**, *114*, 131−142.
(27) Leeuwner, M. J.; Patra, A.; Wilkinson, D. P.; Gyenge, E. L. Graphene and reduced graphene oxide based microporous layers for high-performance proton-exchange membrane fuel cells under varied humidity operation. *J. Power Sources* **2019**, *423*, 192−202.
(28) Ramesha, G. K.; Sampath, S. Electrochemical Reduction of Oriented Graphene Oxide Films: An in Situ Raman Spectroelectrochemical Study. *J. Phys. Chem. C* **2009**, *113* (19), 7985−7989.
(29) Wu, J.-B.; Lin, M.-L.; Cong, X.; Liu, H.-N.; Tan, P.-H. Raman spectroscopy of graphene-based materials and its applications in related devices. *Chem. Soc. Rev.* **2018**, *47* (5), 1822−1873.
(30) Wu, Y.; Charlesworth, L.; Maglaya, I.; Idros, M. N.; Li, M.; Burdyny, T.; Wang, G.; Rufford, T. E. Mitigating Electrolyte Flooding for Electrochemical CO2 Reduction via Infiltration of Hydrophobic Particles in a Gas Diffusion Layer. *ACS Energy Lett.* **2022**, *7* (9), 2884−2892.
(31) Pham, T. H. M.; Zhang, J.; Li, M.; Shen, T.-H.; Ko, Y.; Tileli, V.; Luo, W.; Züttel, A. Enhanced Electrocatalytic CO2 Reduction to C2+ Products by Adjusting the Local Reaction Environment with Polymer Binders. *Adv. Energy Mater.* **2022**, *12* (9), 2103663.
(32) Schwamb, T.; Burg, B. R.; Schirmer, N. C.; Poulikakos, D. An electrical method for the measurement of the thermal and electrical conductivity of reduced graphene oxide nanostructures. *Nanotechnology* **2009**, *20* (40), 405704.
(33) Wu, Y.; Garg, S.; Li, M.; Idros, M. N.; Li, Z.; Lin, R.; Chen, J.; Wang, G.; Rufford, T. E. Effects of microporous layer on electrolyte flooding in gas diffusion electrodes and selectivity of CO2 electrolysis to CO. *J. Power Sources* **2022**, *522*, 230998.
(34) Leonard, M. E.; Clarke, L. E.; Forner-Cuenca, A.; Brown, S. M.; Brushett, F. R. Investigating Electrode Flooding in a Flowing Electrolyte, Gas-Fed Carbon Dioxide Electrolyzer. *ChemSuschem* **2020**, *13* (2), 400−411.
(35) Wei, P.; Li, H.; Lin, L.; Gao, D.; Zhang, X.; Gong, H.; Qing, G.; Cai, R.; Wang, G.; Bao, X. CO2 electrolysis at industrial current densities using anion exchange membrane based electrolyzers. *Sci. China: chem.* **2020**, *63* (12), 1711−1715.
(36) Zhuang, T.-T.; Pang, Y.; Liang, Z.-Q.; Wang, Z.; Li, Y.; Tan, C.-S.; Li, J.; Dinh, C. T.; De Luna, P.; Hsieh, P.-L.; et al. Copper nanocavities confine intermediates for efficient electrosynthesis of C3 alcohol fuels from carbon monoxide. *Nat. Catal.* **2018**, *1* (12), 946−951.
(37) Fan, L.; Xia, C.; Zhu, P.; Lu, Y.; Wang, H. Electrochemical CO2 reduction to high-concentration pure formic acid solutions in an all-solid-state reactor. *Nat. Commun.* **2020**, *11* (1), 3633.
(38) Garg, S.; Li, M.; Wu, Y.; Nazmi Idros, M.; Wang, H.; Yago, A. J.; Ge, L.; Wang, G. G. X.; Rufford, T. E. Understanding the Effects of Anion Interactions with Ag Electrodes on Electrochemical CO2 Reduction in Choline Halide Electrolytes. *ChemSuschem* **2021**, *14* (12), 2601−2611.
(39) Dupont, M.; Hollenkamp, A. F.; Donne, S. W. Electrochemically active surface area effects on the performance of manganese dioxide for electrochemical capacitor applications. *Electrochim. Acta* **2013**, *104*, 140−147.
(40) Jiang, K.; Huang, Y.; Zeng, G.; Toma, F. M.; Goddard, W. A., III; Bell, A. T. Effects of Surface Roughness on the Electrochemical Reduction of CO2 over Cu. *ACS Energy Lett.* **2020**, *5* (4), 1206−1214.
(41) Nguyen, D. L. T.; Lee, C. W.; Na, J.; Kim, M.-C.; Tu, N. D. K.; Lee, S. Y.; Sa, Y. J.; Won, D. H.; Oh, H.-S.; Kim, H.; et al. Mass Transport Control by Surface Graphene Oxide for Selective CO Production from Electrochemical CO2 Reduction. *ACS Catal.* **2020**, *10* (5), 3222−3231.

https://doi.org/10.1021/acsami.4c09095
ACS Appl. Mater. Interfaces 2024, 16, 56967−56974

(42) Ma, T.; Fan, Q.; Li, X.; Qiu, J.; Wu, T.; Sun, Z. Graphene-based materials for electrochemical CO2 reduction. *J. CO2 Util.* **2019**, *30*, 168−182.
(43) Zheng, T.; Jiang, K.; Ta, N.; Hu, Y.; Zeng, J.; Liu, J.; Wang, H. Large-Scale and Highly Selective CO2 Electrocatalytic Reduction on Nickel Single-Atom Catalyst. *Joule* **2019**, *3* (1), 265−278.
(44) Jiang, K.; Siahrostami, S.; Zheng, T.; Hu, Y.; Hwang, S.; Stavitski, E.; Peng, Y.; Dynes, J.; Gangisetty, M.; Su, D.; et al. Isolated Ni single atoms in graphene nanosheets for high-performance CO2 reduction. *Energy Environ. Sci.* **2018**, *11* (4), 893−903.
(45) Chai, R.; Liu, Y.; Wang, J.; Liu, Q.; Rui, Z. CO2 utilization and sequestration in Reservoir: Effects and mechanisms of CO2 electrochemical reduction. *Appl. Energy* **2022**, *323*, 119584.
(46) Choi, J.; Mun, J.; Wang, M. C.; Ashraf, A.; Kang, S.-W.; Nam, S. Hierarchical, Dual-Scale Structures of Atomically Thin MoS2 for Tunable Wetting. *Nano Lett.* **2017**, *17* (3), 1756−1761.
(47) Yun, T.; Lee, G. S.; Choi, J.; Kim, H.; Yang, G. G.; Lee, H. J.; Kim, J. G.; Lee, H. M.; Koo, C. M.; Lim, J.; et al. Multidimensional Ti3C2Tx MXene Architectures via Interfacial Electrochemical Self-Assembly. *ACS Nano* **2021**, *15* (6), 10058−10066.

https://doi.org/10.1021/acsami.4c09095
ACS Appl. Mater. Interfaces 2024, 16, 56967−56974